Raman peak shifts by applied magnetic field in InSb/$Al_xIn_{1-x}Sb$ superlattices

Materials Research Express

PAPER

Raman peak shifts by applied magnetic field in InSb/$Al_xIn_{1-x}Sb$ superlattices

Matasit Chikumpa[1], Zon[1], Supachok Thainoi[1], Suwit Kiravittaya[2], Aniwat Tandaechanurat[3], Noppadon Nuntawong[4], Suwat Sopitpan[4], Visittapong Yordsri[4], Chanchana Thanachayanont[4], Songphol Kanjanachuchai[1], Somchai Ratanathammaphan[1] and Somsak Panyakeow[1]

[1] Semiconductor Devices Research Laboratory, Department of Electrical Engineering, Faculty of Engineering, Chulalongkorn University, Bangkok, Thailand
[2] Advanced Optical Technology Laboratory, Department of Electrical and Computer Engineering, Faculty of Engineering, Naresuan University, Phitsanulok, Thailand
[3] International School of Engineering (ISE), Faculty of Engineering, Chulalongkorn University, Bangkok, Thailand
[4] National Science and Technology Development Agency (NSTDA), Pathumthani 12120, Thailand

E-mail: s_panyakeow@yahoo.com

Keywords: InSb/AlInSb, superlattices, molecular beam epitaxy, Raman spectroscopy, magnetic effect

OPEN ACCESS

RECEIVED
1 August 2020

REVISED
30 September 2020

ACCEPTED FOR PUBLICATION
2 October 2020

PUBLISHED
14 October 2020

Abstract

InSb/$Al_xIn_{1-x}Sb$ superlattices (SLs) are grown by molecular beam epitaxy on (001) InSb substrate and Raman scattering spectroscopy of the samples under magnetic field is investigated. Al contents in AlInSb of the samples are varied. All samples are characterized by atomic force microscopy (AFM), X-ray diffraction and Raman scattering spectroscopy. The Raman spectroscopy is done by using excitation laser with 633 nm wavelength and 2 μm beam spot under applied magnetic field from 0 to 170 mT. Both TO and LO Raman peaks from InSb are detected from all samples. There are Raman peak shift of both TO and LO by applied magnetic field. Stronger magnetic effect is found in LO than TO phonon modes. We attribute this effect to the symmetry breaking of the InSb/AlInSb interfaces since the observed roughness of the top InSb layer can qualitatively correlate with the shift.

1. Introduction

In the last decades, III-V compound superlattices (SLs) and quantum nanostructures have been widely investigated as they are promising structures for novel electronic and optoelectronic device applications [1, 2]. Among them, antimonide-based material systems namely InSb, GaSb, AlSb, InGaSb, AlGaSb have been explored for their basic properties of various substrates (GaAs, InAs, GaSb, and InSb) [3–14]. Structural characteristics of both nearly lattice-matched such as InAs/GaSb and many mismatched systems are reported along with their fabrication details as they are the prerequisites for the successful realization of novel nano-devices.

Concerning the device applications of InSb-based systems, InSb/AlInSb SLs or quantum nanostructures can be utilized for realizing high performance optoelectronic devices operating in infrared wavelength range [8, 9, 15–22]. It has also been demonstrated that InSb can be used as Hall bar for magnetic field sensing since the room temperature (RT) electron mobility in InSb is highest among all III-V compounds [23–25]. Typically, two-dimensional electron gas is formed in the high-electron mobility structure based on this material. However, the magneto-optical properties of InSb/AlInSb SLs in visible range have not been well investigated.

Recently, we have observed a small but noticeable Raman scattering peak shifts of samples containing nanostructures [9]. In another work [26], the Raman peak shift is observed in free-standing InSb nanowire sample. The observed results for InSb nanowires [26] and nano-stripes [9] are less obvious as compared to other material systems [27, 28]. We thus investigate the InSb/AlInSb SLs. In this work, we report on the realization and Raman peak shifts of InSb/$Al_xIn_{1-x}Sb$ SLs. The Al content x is varied and the shifts of both LO and TO peaks are observed in all Al-contained samples. We have qualitatively explained the origin of these shifts to the

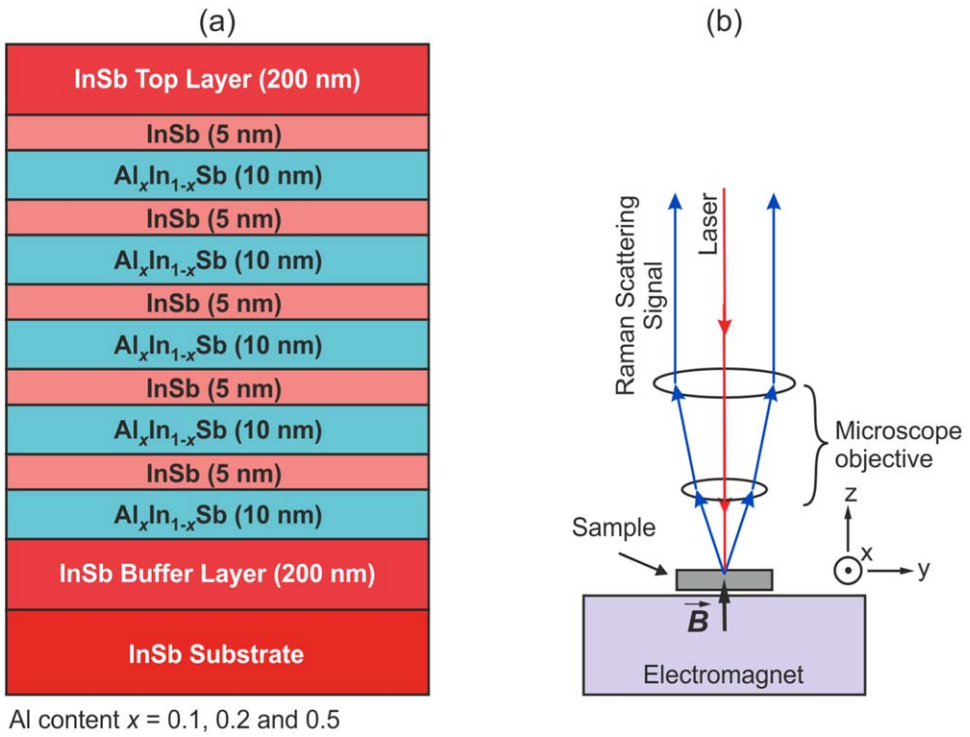

Figure 1. (a) Schematic diagram of the InSb/$Al_xIn_{1-x}Sb$ SL structure grown on (001) InSb substrate. One period of SL structure consists of 5-nm-thick InSb and 10-nm-thick AlInSb layers. (b) Schematic view of the sample and electromagnet arrangement in the micro-Raman spectroscopy setup. The external magnetic field $\vec{B}$ is applied along *z* axis. The red line with arrows showing the 633-nm laser using to excite the Raman signals. The blue lines with arrows show the Raman scatterings from the sample. The signal is collected by the 50 × objective lens.

interface inhomogeneity of the InSb/AlInSb interface as the roughness of InSb top layer can be correlated to the interface.

2. Sample preparation

InSb/$Al_xIn_{1-x}Sb$ ×5 SL samples are grown on (001) InSb substrates by molecular beam epitaxy (MBE RIBER Compact 21TM) equipped with an antimony (Sb) valved cracker cell. The In and Al sources are conventional effusion cells. The overall growth process was monitored *in situ* by reflection high energy electron diffraction (RHEED) observation. Prior to the growth, the substrate is pre-heated at 200 °C for 1 h in the preheating chamber. After preheating, it is transferred into the MBE growth chamber and the de-oxidation process is performed. By RHEED observation, the surface is de-oxidized at 380 °C. To minimize the surface roughness after de-oxidation process, 200 nm thick InSb buffer layer with In growth rate of 0.12 monolayer per second (ML/s) is grown on the InSb substrate at de-oxidized temperature 380 °C. Then, $Al_xIn_{1-x}Sb$ (10 nm) layer is grown and followed by InSb (5 nm) layer for complete one period of InSb/AlInSb SL. The Al content *x* in AlInSb is varied from 0.1 to 0.2 and 0.5 adjusted by the temperature of Al effusion cell in the range of ~1010 to ~1120 °C for the targeted amount of Al composition. The SL active region is composed of five periods-InSb (5 nm)/AlInSb (10 nm). Finally, 200-nm-thick InSb layer is grown at the topmost of the SL structure as the capping layer. The substrate temperature and In growth rate are fixed at 380 °C, 0.12 ML s^{-1} for overall MBE growth process. The schematic diagram of InSb/AlInSb SL structure is shown in figure 1(a).

The surface morphology of the grown samples is characterized by the atomic force microscopy (AFM, Seiko SPA-400) in dynamic force mode in air. Crystalline quality, layer thickness and the lattice parameter variation relating to III-V compound composition are probed by an X-ray diffractometer (HR-XRD Rigaku TTRAX III) operated at 50 kV. The Raman spectroscopy (Reinshaw inVia^{TM}) is performed by employing 633-nm excitation laser at RT. Figure 1(b) shows the arrangement of the sample and electromagnet in the micro-Raman spectroscopy setup. In order to investigate the effect of magnetic field on the Raman spectra, the external magnetic field $\vec{B}$ is increased from 0 to 32 , 64 , 89 , 122 , 144 and 170 millitesla (mT). The magnetic field is controlled by the applied voltage to an electromagnet. Calibration with a commercial magnetometer is performed before and after the experiment. The magnetic field $\vec{B}$ is applied in *z* direction.

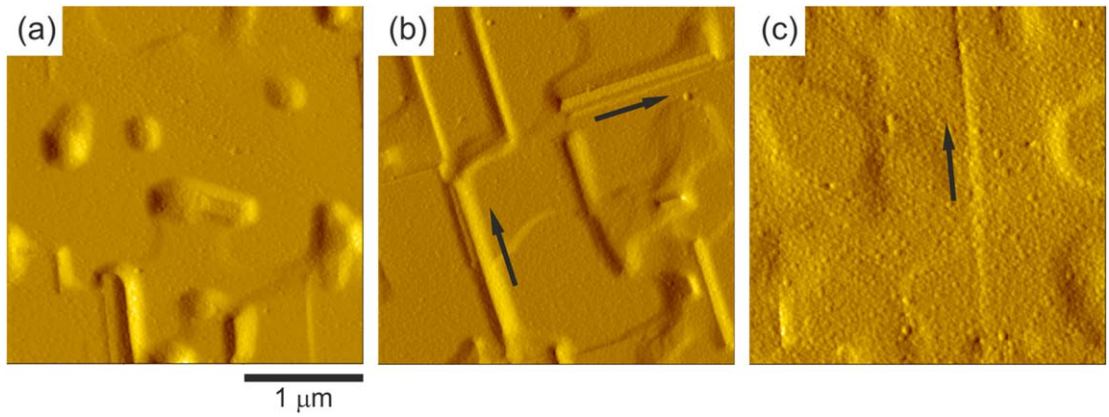

Figure 2. 3 × 3 μm^2 AFM images of top InSb layers grown on InSb/$Al_xIn_{1-x}Sb$ SL having Al contents x of (a) 0.1, (b) 0.2 and (c) 0.5. The arrows show the elongated trends observing on the surface.

3. Results and discussion

The surface morphology of the topmost InSb layer is observed by AFM. Figures 2(a)–(c) shows the typical InSb surfaces from the samples having Al content $x = 0.1, 0.2$, and 0.5. Holes and elongated trends are observed on the surface of the sample with $x = 0.1$. The similar trends get longer and show densely on the $x = 0.2$ sample. The roughness of $x = 0.5$ sample gets higher showing corrugated and stepped surface. The RMS roughness values of the top InSb surfaces of the samples with $x = 0.1, 0.2$ and 0.5 are 1.33, 2.09 and 2.42 nm, respectively, by probing the 1 × 1 μm^2 surface area. This roughness can be related to the interface roughness of underneath InSb/AlInSb SLs and it might relate to the degree of Raman peak shifts, which are shown below.

HR-XRD analysis is carried out to investigate the crystalline quality, layer thickness and III-V compound composition in the InSb/$Al_xIn_{1-x}Sb$ SL structure. The samples are diffracted by x-ray beam with wavelength of 1.5406 Å (Cu Kα_1) at 0.02° step. Figure 3(a) shows the overall XRD patterns in log (normalized) scale of the three samples with various x and InSb substrate (reference) at the diffraction angle 2θ range between 20° and 80°. InSb peaks from (200) reflection at $2\theta \sim 28°$ and (400) reflection at $2\theta \sim 57°$ are observed [11, 17]. Magnified view of XRD patterns are shown in figure 3(b). The (400) reflection peak of InSb is observed at $2\theta \sim 56.79°$. The reflections at $2\theta \sim 57°$–59° can be assigned to the central diffraction peaks from mixtures of epitaxial InSb and $Al_xIn_{1-x}Sb$ layers. The diffraction angle 2θ calculation is done by using typical Bragg Law. To evaluate the behaviour of material composition in the investigated SLs, we calculate the diffraction angle 2θ of SL in two models; one for AlInSb peak and one for InSb/AlInSb mixture peak. The calculated and experimental results are described in table 1. The experimental results of central 2θ reflections are extracted by the function of Lorentz fit. The result from XRD shows monotonic shift and broadening of the InSb/$Al_xIn_{1-x}Sb$ peak when the aluminium content increases (from 0.1 to 0.5). The former is due to the increase of the Al content x while the latter is from the roughness increment. This deliberate growth of SL with low structural quality (high roughness) is done in order to probe the magnetic field induced Raman peak shift, which is shown below.

The Raman spectroscopy is performed to study the strain characteristics of the InSb/AlInSb SL structure, and the relation between the magnetic field B and the Raman frequency shift. To investigate the effect of external applied B on the Raman spectrum, B is increased from 0 to 32, 64, 89, 122, 144 and 170 mT while the excitation laser wavelength is fixed at 633 nm. B is aligned along in the z direction. The beam spot size of excitation laser is ~2 μm by employing the 50 × objective lens, and the signal is scanned with the acquisition time of 20 s. Figure 4(a) shows the Raman scattering spectrum of SL ($x = 0.1$) measured without B. The three peaks corresponding to the Sb cluster, first and second order InSb are observed at ~140, 170–200 and 370–385 cm^{-1}, respectively [9, 11–14, 29]. Since the vicinity of laser beam spot is ~2 μm, B interacting with laser beam excitation is limited. With limited area of interaction, however, the evolution of the Raman shift as the function of B is occurred in all samples as shown in figures 4(b)–(d). The strong first order InSb peak is focussed to study the Raman peak shift. When B increases from 0 to 170 mT, the blue-shift of transverse optical (TO) and longitudinal optical (LO) phonon peaks of InSb is observed. The broad Raman scattering features at lower values of B is the resultants from the contributing of TO and LO phonon peaks, and the LO phonon peak is getting stronger and clearly split from TO mode at higher values of B. We speculate that the lattice vibration or polarization of LO phonons is more strongly affected by the external magnetic field than that of TO phonons.

Raman frequency shift as the function of B is summarized as shown in figure 5 for the investigated samples. The peak-positions of LO and TO phonon modes are extracted by fitting with the Gaussian function. The values

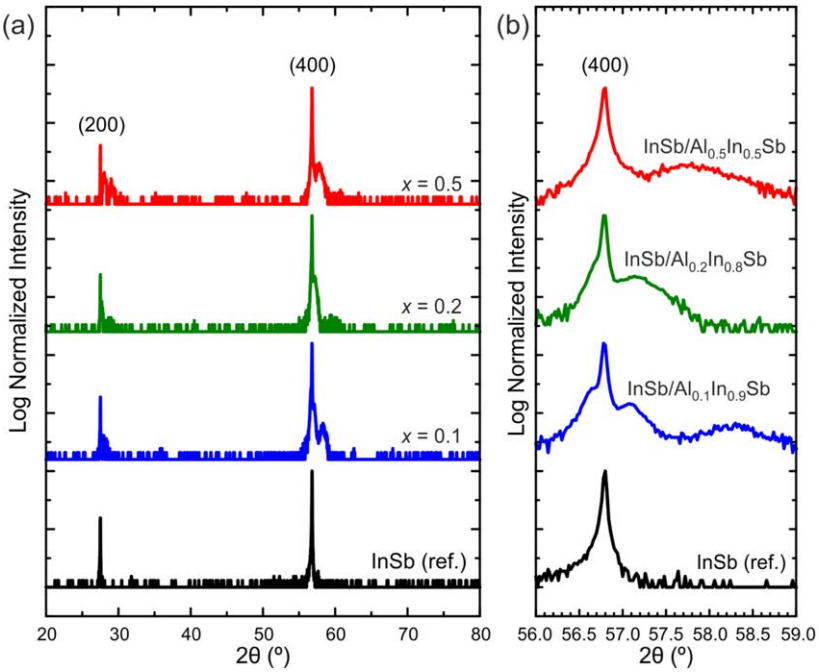

Figure 3. HR-XRD patterns of ω-2θ scan around InSb (200) and (400) reflections for InSb/$Al_xIn_{1-x}Sb$ SL ($x = 0.1, 0.2, 0.5$) between the diffraction angle 2θ of (a) 20°–80° and (b) 56–59° (Magnified view). The lowest XRD pattern of InSb substrate is plotted as the reference (black line). The patterns are plotted in logarithmic scale and shifted upward for clarity.

Table 1. Comparison of calculated and experimental X-ray diffraction angle 2θ of InSb/$Al_xIn_{1-x}Sb$ superlattices with different Al content x.

	Calculation						
Al content x	$Al_xIn_{1-x}Sb$ peak			InSb/$Al_xIn_{1-x}Sb$ peak			Experiment
	$2\theta_-$ (°)	$2\theta_0$ (°)	$2\theta_+$ (°)	$2\theta_-$ (°)	$2\theta_0$ (°)	$2\theta_+$ (°)	$2\theta_0$ (°)
0.1	56.45	57.12	57.79	56.34	57.01	57.68	57.12
0.2	56.78	57.45	58.13	56.56	57.23	57.90	57.23
0.5	57.81	58.48	29.16	57.23	57.90	58.58	57.85

$2\theta_-$ = first satellite peak at negative angle.
$2\theta_0$ = central diffraction angle.
$2\theta_+$ = first satellite peak.

of (LO and TO) phonon peak shifts for InSb/AlInSb SLs with $x = 0.1, 0.2$ and 0.5 are (2.19, 1.59), (2.95, 2.24), and (4.16, 2.03) cm^{-1}, respectively. The slope of shifting data indicates the sensitivity of magnetic effect of each sample. The samples with $x = 0.1$ and 0.2 show similar results with nearly the same slope and discrepancy among the LO and TO lines. The general concept of the Raman frequency shift of the optical phonons, $\Delta\omega$, by the external applied magnetic field, B, can be simply expressed as

$$\Delta\omega = \gamma B,$$

where, γ is an empirical constant (in the unit of cm^{-1}/mT). The experimental results indicate that the γ_{LO} is larger at SL with $x = 0.5$, which can be related to the different lattice vibration due to the lattice parameter variation by increasing x. In this work, the origin of these shifts can be qualitatively explained as the interface inhomogeneity of the InSb/AlInSb interface correlating to the surface corrugation of InSb top layer. Since perfect non-magnetic crystals such as III-V compound semiconductors do not show a magnetic field induced Raman shift [30]. Further theoretical considerations as well as explicit atomistic calculations are still needed to proceed for developing a complete understanding of this phenomenon [30, 31].

Comparison on the Raman peak positions of the three SL samples with various x at $B = 0$ up to 170 mT, the red-shift of the Raman scatterings is revealed as x increases. The fitted TO and LO peak positions of the three SLs with $x = 0.1, 0.2$ and 0.5 at $B = 0$ mT are obtained at (178.75, 185.79), (176.82, 185.05) and (176.63, 183.50) cm^{-1}, respectively. The TO and LO peaks are shifted by 1.93 cm^{-1} and 0.74 cm^{-1} when x increases from 0.1 to 0.2, and 0.19 cm^{-1} and 1.55 cm^{-1} when x increases from 0.2 to 0.5, respectively. The possible explanation for

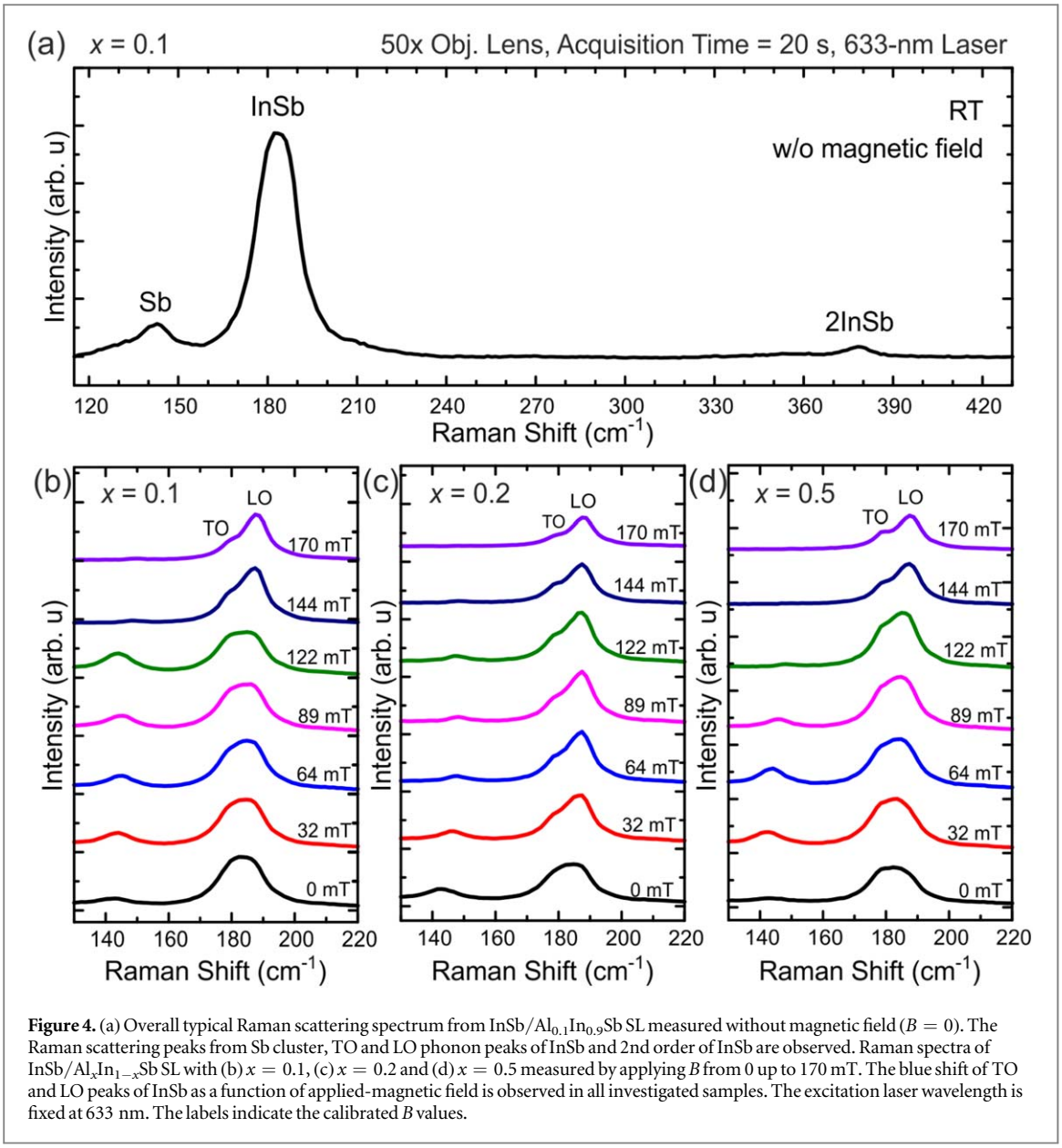

Figure 4. (a) Overall typical Raman scattering spectrum from InSb/$Al_{0.1}In_{0.9}Sb$ SL measured without magnetic field ($B = 0$). The Raman scattering peaks from Sb cluster, TO and LO phonon peaks of InSb and 2nd order of InSb are observed. Raman spectra of InSb/$Al_xIn_{1-x}Sb$ SL with (b) $x = 0.1$, (c) $x = 0.2$ and (d) $x = 0.5$ measured by applying B from 0 up to 170 mT. The blue shift of TO and LO peaks of InSb as a function of applied-magnetic field is observed in all investigated samples. The excitation laser wavelength is fixed at 633 nm. The labels indicate the calibrated B values.

these shifts is that the dislocations generated by the relaxation of misfit strain are eliminated at the interfaces in the SL. The nearby areas have both the compressive and tensile strained regions. In our case, the red-shift of the Raman phonon peaks can be attributed to the induced tensile strain at the InSb/AlInSb interfaces manipulated by the Al composition in the ternary compound AlInSb.

4. Summary

InSb/$Al_xIn_{1-x}Sb$ SLs with various Al contents ($x = 0.1, 0.2$ and 0.5) have been prepared on InSb substrates by MBE The surface corrugation of top InSb layer is qualitatively analysed by AFM. The sample with x = 0.5 gets most roughening surface among the investigated samples. XRD measurement exhibits the reflections from InSb and the InSb/$Al_xIn_{1-x}Sb$ mixture. By comparing with the calculated values, the material intermixing occurs at the interfaces of SL, and the diffraction peaks are mainly observed from the InSb/$Al_xIn_{1-x}Sb$ mixture. Micro-Raman spectroscopy accompanying with external applied magnetic field B reveals that the influence of magnetic field on the InSb/$Al_xIn_{1-x}Sb$ SL structure. InSb/$Al_{0.5}In_{0.5}Sb$ SL has the highest magnetic response of phonons to the applied B. The clear blue-shift of TO and LO Raman phonon scatterings of SL is observed when $B = 0$ up to 170 mT. This can be implied to the dissymmetry behaviour of the InSb/AlInSb interfaces which is correlated to the surface roughness of the top InSb layer. Moreover, the red-shifts of TO and LO Raman phonon peaks reveal the relaxation of tensile strain at the interfaces induced by higher Al composition.

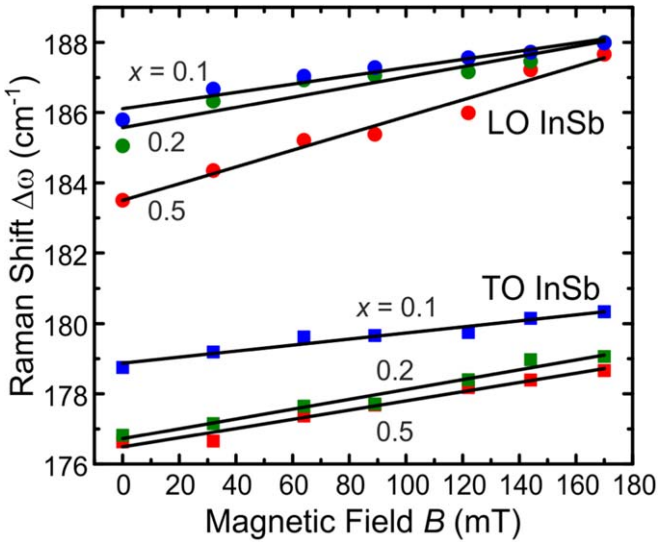

Figure 5. The linear fitting curves of the LO and TO peak shifts $\Delta\omega$ by varying applied magnetic field $\vec{B}$. The Raman scattering frequencies as a function of $\vec{B}$ for InSb/$Al_xIn_{1-x}Sb$ SL with $x = 0.1, 0.2$ and 0.5 are represented by blue, green and red dots.

Acknowledgments

This research was financially supported by the Research Chair Grant, the National Science and Technology Development Agency (NSTDA), Thailand (Contract No. FDA-CO-2558-1407-TH), the Asian Office of Aerospace Research and Development (AOARD) Grant, co-funded with the Office of Naval Research Global (ONRG) under Grant No. FA 2386-16-1-4003, Thailand Research Fund (Contract No. DPG5380002), NANOTEC, NSTDA, Thailand (Contract No. RES-50-016-21-016), and Chulalongkorn University. Ms. Zon acknowledges support from the Ratchadaphiseksomphot Fund for Postdoctoral Fellowships of Chulalongkorn University.

ORCID iDs

Zon https://orcid.org/0000-0003-1998-6482
Suwit Kiravittaya https://orcid.org/0000-0003-0609-5445
Songphol Kanjanachuchai https://orcid.org/0000-0003-4622-4176
Somsak Panyakeow https://orcid.org/0000-0002-8618-1839

References

[1] Böer K W and Pohl U W 2018 *Semiconductor Physics* 1st ed. (Cham, Switzerland: Springer International Publishing) (https://doi.org/10.1007/978-3-319-69150-3)
[2] Steiner T (ed) 2004 *Semiconductor nanostructures for optoelectronic applications* (Boston, London: Artech House)
[3] Brar B and Kroemer H 1998 Hole transport across the (Al, Ga) (As, Sb) barrier in InAs–(Al, Ga) (As, Sb) heterostructures *Journal of Applied Physics* **83** 894
[4] Bennett B R, Magno R, Boos J B, Kruppa W and Ancona M G 2005 Antimonide-based compound semiconductors for electronic devices: a review *Solid-State Electronics* **49** 1875
[5] Liu C, Li Y and Zeng Y 2010 Progress in Antimonide based III-V compound semiconductors and devices *Engineering* **2** 617
[6] Razeghi M 2003 Overview of antimonide based III-V semiconductor epitaxial layers and their applications at the center for quantum devices *The European Physical Journal Applied Physics* **23** 149
[7] Razeghi M, Huang E K, Nguyen B-M, Ramezani-Darvish S, Pour S A, Chen G, Haddadi A and Hoang M-A 2011 Recent advances in high-performance antimonide-based superlattice FPAs *Proceeding of SPIE 8012, Infrared Technology and Applications* **XXXVII** 80120T
[8] Okamoto A, Yoshida T, Muramatsu S and Shibasaki I 1999 Magneto-resistance effect in InSb thin film grown using molecular beam epitaxy *Journal of Crystal Growth* **201** 765
[9] Lekwongderm P *et al* 2019 Study on Raman spectroscopy of InSb nano-stripes grown on GaSb substrate by molecular beam epitaxy and their Raman peak shift with magnetic field *Journal of Crystal Growth* **512** 198
[10] Yong L *et al* 2020 MBE growth of high quality AlInSb/GaSb compound buffer layers on GaAs substrates *Optical and Quantum Electronics* **52** 138
[11] Webb J B, Lockwood D J and Gnezdilov V P 1994 Magnetron sputter epitaxy and characterization of InSb/$In_{1-x}Al_xSb$ strained layer superlattices *Journal of Crystal Growth* **137** 405
[12] Gnezdilov V P, Lockwood D J and Webb J B 1993 Phonon Rarnan scattering in InSb/$In_{1-x}Al_x$Sbstrained-layer superlattices *Physical Review B* **48** 11228–33

[13] Gnezdilov V P, Lockwood D J and Webb J B 1993 Resonant Raman scattering in an InSb/$In_{1-x}Al_xSb$ strained-layer superlattice and in $In_{1-x}Al_xSb$ epilayers on InSb *Physical Review B* **48** 11234
[14] Thainoi S, Kiravittaya S, Poempool T, Zon, Nuntawong N, Sopitpan S, Kanjanachuchai S, Ratanathammaphan S and Panyakeow S 2017 Molecular beam epitaxy growth of InSb/GaAs quantum nanostructures *Journal of Crystal Growth* **477** 30
[15] Sandhu A, Sanbonsugi H, Shibasaki I, Abe M and Handa H 2004 High sensitivity InSb ultra-thin film micro-Hall sensors for bioscreening applications *Japanese Journal of Applied Physics* **43** (Part 2) 7A
[16] Heremans J, Partin D L, Thrush C M and Green L 1993 Narrow-gap semiconductor magnetic- field sensors and applications *Semiconductor Science and Technology* **8** 1S
[17] Ueno K, Camargo E G, Katsumata T, Goto H, Kuze N, Kangawa Y and Kakimoto K 2013 InSb mid-infrared photon detector for room-temperature operation *Japanese Journal of Applied Physics* **52** 9R
[18] Bakarov A K, Gutakovskii A K, Zhuravlev K S, Kovchavtsev A P, Toropov A I, Burlakov I D, Boltar K O, Vlasov P V and Lopukhin A A 2017 MBE-Grown InSb Photodetector Arrays *Solid State Electronics* **87** 900
[19] Srisinsuphya P *et al* 2019 InSb/InAs quantum nano-stripes grown by molecular beam epitaxy and its photoluminescence at mid-infrared wavelength *Journal of Crystal Growth* **514** 36
[20] Kunets V P, Easwaran S, Black W T and Guzun D 2009 InSb quantum-well-based micro-Hall devices: potential for pT detectivity *IEEE Transactions on Electron Devices* **56** 683
[21] Chadda S, Datye A and Ralph Dawson L 1993 Microstructural evaluation of strained multilayer InAsSb/InSb infrared detectors by transmission electron microscopy *Journal of Applied Physics* **73** 4232
[22] Bakarov A K, Gutakovskii A K, Zhuravlev K S, Kovchavtsev A P, Toropov A I, Burlakov I D, Boltar K O, Vlasov P V and Lopukhin A A 2017 MBE-Grown InSb photodetector arrays *Technical Physics* **62** 915
[23] Vurgaftman I, Meyer J R and Ram-Mohan L R 2001 Band parameters for III-V compound semiconductors and their alloys *Journal of Applied Physics* **89** 5815
[24] Nilsson H A, Caroff P, Thelander C, Larsson M, Wagner J B, Wernersson L-E, Samuelson L and Xu H Q 2009 Giant level-dependent g factors in InSb nanowire quantum dots *Nano Letters* **9** 3151–6
[25] Isaacson R A 1968 Electron Spin Resonance in n-Type InSb *Physical Review* **169** 312
[26] Hossain M I, Atulasimha J and Bandyopadhyay S 2015 Raman spectroscopy studies of phonons in a nanowire subjected to a magnetic field *IEEE Nanotechnology Materials and Devices Conference* p. 1–3
[27] Li J-M, Huan A C H, Wang L, Du Y-W and Feng D 2000 Interface effects on magnetoresistance and magnetic-field-reduced Raman scattering in magnetite *Physical Review B* **61** 6876
[28] Li J-M, Huan A C H, Wang L, Du Y-W, Feng D and Shen Z X 2001 Magnetic-field-tunable charge carrier localization in sintered polycrystalline $La_{0.75}Ca_{0.25}MnO_3$ *Physical Review B* **63** 024416
[29] Narabadeesuphakorn P *et al* 2018 Twin InSb/GaAs quantum nano-stripes: growth optimization and related properties *Journal of Crystal Growth* **487** 40
[30] Anastassakis E 1980 Ch. 3 Morphic Effects in Lattice Dynamics *Dynamical Properties of Solids edited by Horton and Maradudin* (New York: North-Holland Publishing Company)
[31] Anastassakis E, Burstein E, Maradudin A A and Minnick R 1972 Morphic effects—IV. Effects of an Applied Magnetic Field on the First-Order Photon-Optical Phonon Interactions in Non-Magnetic Crystals *Journal of Physics and Chemistry of Solids* **33** 1091